International Journal of Cardiology 286 (2019) 21–28

Contents lists available at ScienceDirect

International Journal of Cardiology

journal homepage: www.elsevier.com/locate/ijcard

In vitro mechanical behavior and in vivo healing response of a novel thin-strut ultrahigh molecular weight poly-L-lactic acid sirolimus-eluting bioresorbable coronary scaffold in normal swine

Yanping Cheng [a], Pawel Gasior [a,c], Kamal Ramzipoor [b], Chang Lee [b], Jenn C. McGregor [a], Gerard B. Conditt [a], Thomas McAndrew [d], Grzegorz L. Kaluza [a], Juan F. Granada [a,d,*]

[a] CRF-Skirball Center for Innovation, Orangeburg, NY, United States of America
[b] Amaranth Medical, Inc., Mountain View, CA, United States of America
[c] 3rd Department of Cardiology, Medical University of Silesia, Katowice, Poland
[d] Cardiovascular Research Foundation, New York, NY, United States of America

ARTICLE INFO

Article history:
Received 21 August 2018
Received in revised form 13 February 2019
Accepted 3 April 2019
Available online 4 April 2019

Keywords:
Bioresorbable scaffolds
Optical coherence tomography
Quantitative coronary angiography
Histopathology

ABSTRACT

Background: New generation bioresorbable scaffolds (BRS) promise to improve the outcomes of current generation BRS technologies by decreasing wall thickness while maintaining structural strength. This study aimed to compare the biomechanical behavior and vascular healing profile of a novel thin-walled (98 μm) sirolimus-eluting ultrahigh molecular weight BRS (Magnitude, Amaranth Medical) to the Absorb everolimus-eluting bioresorbable vascular scaffold (Abbott Vascular).

Methods and results: In vitro biomechanical testing showed lower number of fractures on accelerated cycle testing over time (at 21K cycles = 20.0 [19.0–21.0] in Absorb versus 0.0 [0.0–1.0] in Magnitude-BRS). Either Magnitude (n = 43) or Absorb (n = 22) was implanted in 65 coronary segments of 22 swine. Scaffold strut's coverage was evaluated using serial optical coherence tomography (OCT) analysis. At 14 days, Magnitude-BRS demonstrated a higher percentage of embedded struts (97.7% [95.3, 100.0] compared to Absorb (57.2% [48.0, 76.0], $p = 0.003$) and lower percentage of uncovered struts (0.0% [0.0, 0.0] versus Absorb 5.5% [2.6, 7.7], $p = 0.02$). Also, it showed a lower percent late recoil (−1.02% [−4.11, 3.21] versus 4.42% [−1.10, 8.74], $p = 0.04$) at 28 days. Histopathology revealed comparable neointimal proliferation and vascular healing responses between two devices up to 180 days.

Conclusion: A new generation thin walled (98-μm) Magnitude-BRS displayed a promising biomechanical behavior and strut healing profile compared to Absorb at the experimental level. This new generation BRS platform has the potential to improve the clinical outcomes shown by the current generation BRS.

1. Introduction

The Absorb everolimus-eluting bioresorbable vascular scaffold (BVS, Abbott Vascular) is the most widely studied poly-L-lactic acid (PLLA) based bioresorbable scaffold (BRS) [1,2]. This first generation BRS has an average strut thickness of 157-μm and relies on polymer crystallinity and a high vessel surface area to achieve stent-like mechanical properties. Bench data suggests that this current generation BRS displays limited over-expansion capabilities and structural integrity when exposed to high-loading conditions [3]. Recently published randomized controlled trials suggest that Absorb is associated with an increased risk of late scaffold thrombosis [4–6]. The late biomechanical failure of the device leading to intraluminal dismantling of thick-struts has been suggested as one of the potential mechanisms of scaffold thrombosis in humans [4].

Due to the inherent mechanical limitations of current generation PLLA, the successful development of thin-walled BRS has been challenging. Previous studies have shown that a ultrahigh molecular weight amorphous PLLA-based BRS platform (Amaranth Medical, Mountain View, California) display elongation at break points 10 times higher compared to currently used PLLA and promise to improve the current technical limitations of clinically available BRS [7–9]. In this study, we aimed to evaluate 1) the in vitro mechanical behavior and 2) in vivo strut coverage and vascular healing profile of a novel generation thin-walled (98-μm) sirolimus-eluting amorphous PLLA-based BRS (Magnitude, Amaranth Medical) as compared to Absorb BVS in a porcine coronary artery model.

* Corresponding author at: CRF - Skirball Center for Innovation, Cardiovascular Research Foundation, 8 Corporate Dr., Orangeburg, NY 10962, United States of America.
E-mail address: jgranada@crf.org (J.F. Granada).

https://doi.org/10.1016/j.ijcard.2019.04.012
0167-5273/

2. Methods

2.1. Device description

Similar to previous generation technologies (Fortitude-150 μm and Aptitude-115 μm) [8,9], the BRS tested in this study (Magnitude-98 μm, Amaranth Medical, Mountain View, California) is manufactured using the same polymeric blend coated with a matrix consisting of 1:1 polymer:drug ratio of Sirolimus plus Poly D-Lactide polymer at a concentration of ~96 μg/cm^2. The main features of the Magnitude-BRS are provided in the Online Appendix (Supplementary Fig. 1). In this study, the Magnitude-BRS was compared to the FDA approved, commercially available Absorb everolimus-eluting BRS (Abbott Vascular, Santa Clara, CA).

2.2. In vitro cyclic fatigue testing

The mechanical stability overtime of the Magnitude-BRS (2.5 mm) and Absorb (2.5 mm) was tested under dynamic load conditions (n = 3 for each device). In-vitro cyclic testing method (Supplementary Fig. 2) is provided in the Online Appendix.

2.3. In vivo porcine healing study

The study was approved by the Institutional Animal Care and Use Committee and conducted in compliance with the Guide for the Care and Use of Laboratory Animals formulated by the Institute of Laboratory Animal Resources (National Research Council, 8th edition, 2011 revision). All animals underwent endotracheal intubation and were maintained on a continuous inhalation of 1–3% isoflurane. Either Magnitude (n = 43) or Absorb (n = 22) were implanted in 65 coronary arteries of 22 Yucatan mini swine. In vivo early biomechanics and strut-vessel wall interactions were evaluated longitudinally at post-implantation, 14 and 28 days in 8 animals (12 Magnitude and 8 Absorb) using optical coherence tomography (OCT). The detailed study design and flow-chart are shown in the Online Appendix (Supplementary Fig. 3).

2.4. Quantitative coronary angiography

Quantitative coronary angiography analysis (QCA) was performed using QAngio XA Software™ 7.1.14.0 (Medis Medical Imaging System, Leiden, Netherlands). The reference vessel diameter (RVD) and the minimum lumen diameter (MLD) were automatically calculated by the interpolation method. The percent diameter stenosis (DS) was calculated from the MLD and the RVD. Acute absolute scaffold recoil and percent acute recoil was calculated as previously described [9] (Online Appendix).

2.5. Optical coherence tomography imaging

OCT images were recorded at day 0 post-implantation and at follow-ups using the ILUMIEN PCI Optimization System (St. Jude Medical, St. Paul, MN) following a previously published protocol [10] and the cross-sectional parameters were measured with the commercial software (ILUMIEN OPTIS, St. Jude Medical, St. Paul, MN) as previous described [8,9] at 2-mm axial intervals. In addition, the qualitative embedment analysis for scaffold strut's coverage is provided in the Online Appendix (Supplemental Fig. 4).

2.6. Histological analysis

An independent pathology laboratory (Alizee Pathology, LLC Thurmont, MD) conducted the histo-morphometric analysis. All vessel segments were cut twice serially at ~5 μm and stained with Hematoxylin and Eosin (H & E) and Elastin Trichrome. The following cross-sectional parameters were measured and calculated as previously described [9]: the lumen area, the external elastic lamina (EEL) and internal elastic lamina (IEL), the neointimal thickness and %Area Stenosis. Vessel injury score (0–3), neointimal inflammation (0–4), fibrin deposition (0–3) and neointima maturity (0–3) were semiquantitatively scored for each section as previously descripted [8,9].

2.7. Statistical analyses

Statistical analyses were performed using SAS statistical software (version 9.4; SAS Institute Inc. NC).

Continuous variables were expressed as mean ± SD with the median and interquartile range used for variables with non-normal distributions. A mixed model compared differences between 2 treatments (Magnitude versus Absorb) while accounting for dependent observation over time. Furthermore, this model contained a random effect with compound symmetric covariance structure to account for multiple scaffolds implanted in the same pig. The device, time, and interaction between time and device were modeled as fixed effects. Scheffe's post hoc test was applied to compare differences between time points and differences between treatments at each time point. A nonparametric test was used for those dependent variables with non-normal distributions. All tests were 2-tailed with a Type I error held at 0.05.

3. Results

3.1. In vitro cyclic fatigue study

Under accelerated cycle testing (dynamic conditions), none of the BRS devices tested presented signs of strut fracture at 0 to 3000 cycles. However, in the Absorb group, the number of fractures progressively increased over time (at 5K cycles = 7.5 [3.0–11.5] and 21K cycles = 20.0 [19.0–21.0]). In contrast, in the Magnitude-BRS, no fractures were seen under 11 to 18 K cyclic load conditions and the number of fractures was lower

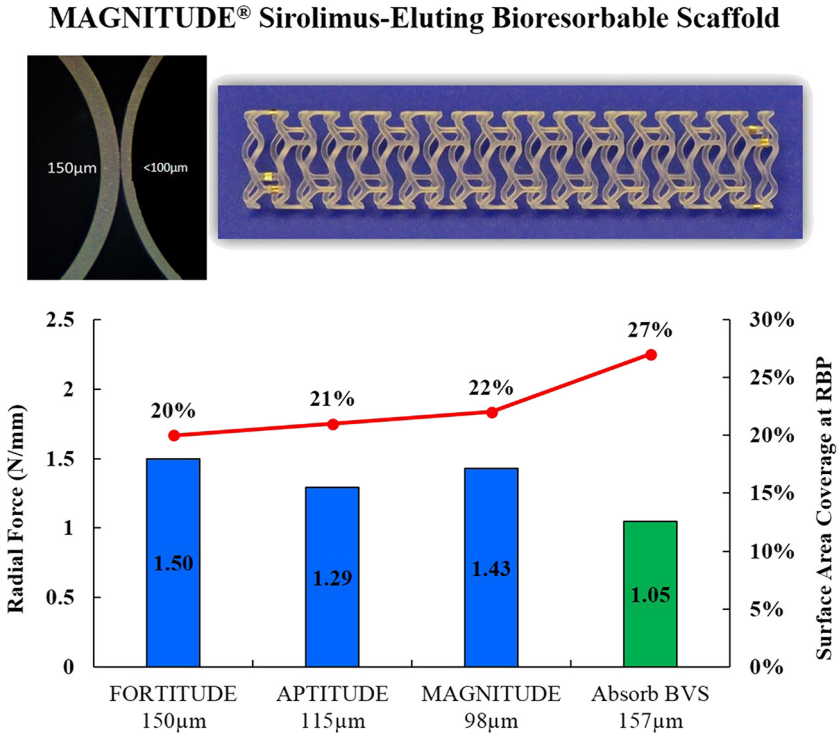

Supplementary Fig. 1. Representative image of the Magnitude sirolimus-eluting bioresorbable scaffold (3.0 × 18 mm) and in vitro radial force and surface area coverage comparisons at rated burst pressure (RBP).

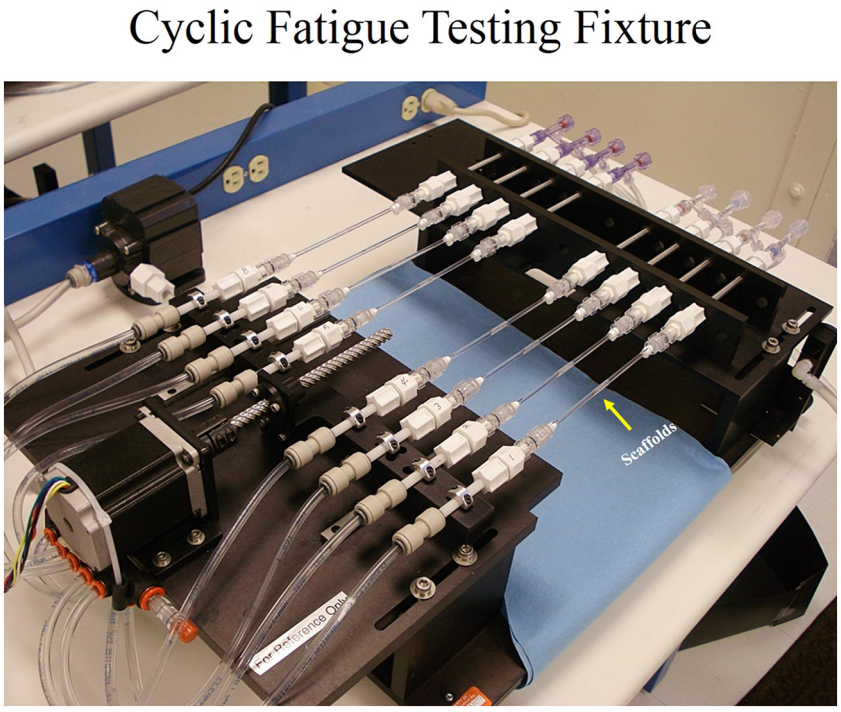

Supplementary Fig. 2. Photo of in-vitro cyclic fatigue testing fixture.

(0.0[0.0–1.0]) compared to Absorb at 21K cycles. Comparative data for both scaffolds are summarized in Supplemental Table 1 in the Online Appendix.

3.2. In vivo porcine healing study

3.2.1. Quantitative coronary angiography analysis

At the time of device implantation, there was no difference in the balloon expansion pressure between the two groups (Magnitude 11.0 ± 4.0 ATM vs Absorb 11.9 ± 4.0 ATM, $p = 0.43$) and the mean balloon-to-artery ratios were comparable between Magnitude and Absorb (Table 1). There were no differences in the post-implant MLD or RVD between two devices. Post-implantation percent (Magnitude: 1.6 ± 4.6% vs. Absorb: 3.6 ± 6.8%, $p = 0.30$) recoil rate was comparable between two scaffolds. There were no significant differences in any of the angiographic variables between both devices at 1, 3 and 6 months (Table 1).

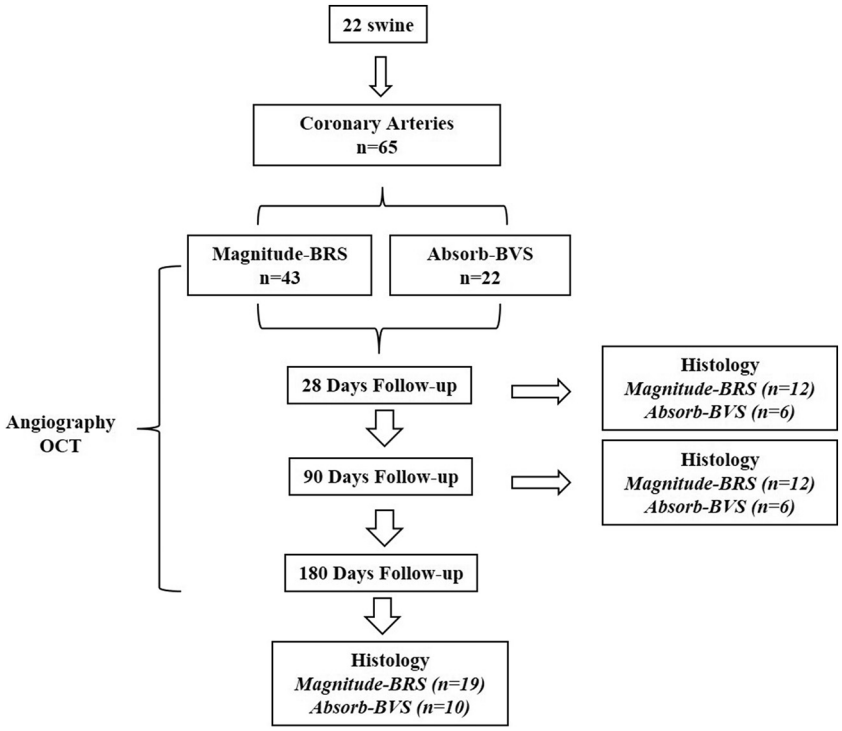

Supplementary Fig. 3. Study flow-chart.

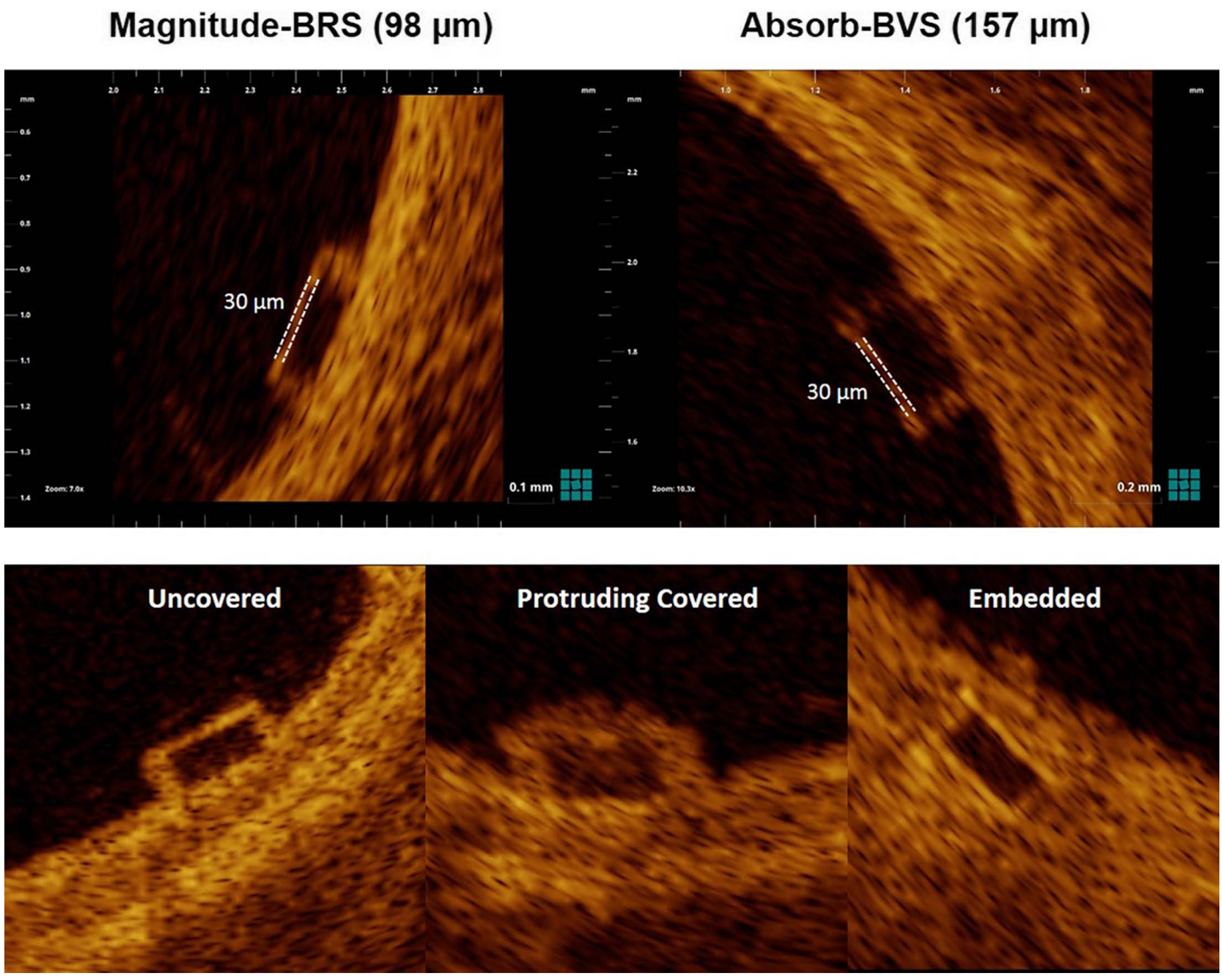

Supplementary Fig. 4. Evaluation of strut coverage using OCT. A: The struts are classified as covered in the presence of a coverage thickness ≥30 μm for both Magnitude-BRS and Absorb-BVS scaffold struts. B: Evaluated struts were assigned to one of the three categories: embedded, protruding covered and uncovered.

3.2.2. OCT coronary healing analysis

At day 0, post-implant OCT indicated that all scaffold struts were fully apposed to the vessel wall with no strut malapposition observed in any of the implanted vessels. No post-dilation was performed. Total 266 cross-sections and 2387 struts were evaluated to sequentially assess biomechanical behavior and short term strut healing response in a subset of animals at 14 and 28 days (Fig. 1A). The percentage of embedded struts was significantly higher at 14 days in the Magnitude-BRS group (Magnitude: 97.7% [95.3, 100.0] vs. Absorb: 57.2% [48.0, 76.0], $p = 0.003$) (Fig. 1B). Conversely, the presence of protruding covered (36.9% [15.6, 45.0]) and uncovered struts (5.5% [2.6, 7.7]) was more commonly observed in Absorb at 14 days and persisted up to 28 days (protruding covered: 1.3% [0.0, 7.5]; uncovered: 0.6% [0.0, 1.9]) (Fig. 1C and D).

OCT data are summarized in Table 2. There were no differences in the post-implant lumen area or scaffold area between two devices. OCT evaluation at 28, 90 and 180 days indicated that there were no significant differences in the lumen area or % AS between two devices at any time point although Absorb displayed significantly higher late absolute recoil and percent recoil rates compared to Magnitude-BRS at 28 and 180 days (Table 2).

3.2.3. Histological analysis

A summary of the histo-morphometric analysis is shown in Table 3. Light microscopic assessment revealed that vascular responses to

Table 1
Angiographic data.

	Magnitude-BRS	Absorb-BVS	*p*
Day 0 (22 animals)	n = 43	n = 22	
Post-RVD (mm)	2.79 ± 0.32	2.85 ± 0.33	0.50
Post-MLD (mm)	2.76 ± 0.27	2.75 ± 0.37	0.83
B:A ratio	1.17 ± 0.09	1.12 ± 0.11	0.06
Day 28 (22 animals)	n = 43	n = 22	
RVD (mm)	2.56 ± 0.32	2.67 ± 0.40	0.30
MLD (mm)	2.18 ± 0.29	2.21 ± 0.40	0.77
% DS	14.39 ± 10.10	17.09 ± 9.92	0.31
LLL (mm)	0.58 ± 0.25	0.54 ± 0.22	0.43
Day 90 (16 animals)	n = 31	n = 16	
RVD (mm)	2.76 ± 0.32	2.87 ± 0.36	0.31
MLD (mm)	2.11 ± 0.30	2.20 ± 0.40	0.47
% DS	23.31 ± 8.35	23.58 ± 9.88	0.93
LLL (mm)	0.63 ± 0.25	0.56 ± 0.28	0.39
Day 180 (10 animals)	n = 19	n = 10	
RVD (mm)	2.92 ± 0.33	2.93 ± 0.26	0.95
MLD (mm)	2.21 ± 0.23	2.08 ± 0.25	0.21
% DS	24.16 ± 5.18	28.76 ± 7.67	0.11
LLL (mm)	0.56 ± 0.21	0.53 ± 0.28	0.77

Mean ± SD. RVD: reference vessel diameter; MLD: minimum lumen diameter; DS: diameter stenosis; LLL: late lumen loss.

Magnitude were comparable with those to Absorb at all time points (Supplemental Fig. 5). At 180 days, evidence of strut stacking or misalignment was observed in 5 of total 57 sections (8.8%) in the Magnitude group, and 2 of total 30 sections (6.7%) in the Absorb group. All these incidental strut discontinuities were focal, fully apposed to the vessel wall and covered with neointima. Neither Magnitude nor Absorb showed evidence of luminal thrombosis of either the main or the side branch of coronary arteries. There were no significant differences in the neointimal thickness, neointimal area and percent area stenosis between two devices at any time points (Table 3). The inflammatory scores were minimal to mild in both groups at all time points (Supplemental Fig. 6). Injury scores were low for both devices and no significant differences were seen in any of the tested time points.

4. Discussion

In this study, we aimed to evaluate the biomechanical properties and healing response of a novel thinned-wall (98-μm) ultra-high molecular weight amorphous PLLA BRS compared to the commercially available Absorb-BVS. The major comparative findings of this study in regard to the tested BRS versus Absorb are: 1) a higher mechanical strength under stress conditions with no in vivo scaffold recoil over time; 2) higher levels of early strut healing, 3) comparable long-term healing and inflammatory responses.

In current generation scaffold, polymer crystallinity and strut thickness determine the mechanical strength of the device. In turn, polymer crystallinity is a result of polymer's molecular weight and manufacturing process of the polymeric tube. For devices using typical PLLA, the total surface area of the device has been increased aiming to compensate losses in radial strength [10]. Novel PLLA formulations promise to improve the biomechanical properties of current generation BRS devices. These polymers have been designed to improve the biomechanical behavior of PLLA by largely depending on the intrinsic material properties instead of purely polymer crystallinity. Our previous studies [7–9] have reported that ultrahigh molecular weight amorphous polymers had higher acute over-expansion capacity and dramatically improved resistance to fracture under static and dynamic conditions. This technological development has allowed the miniaturization of the

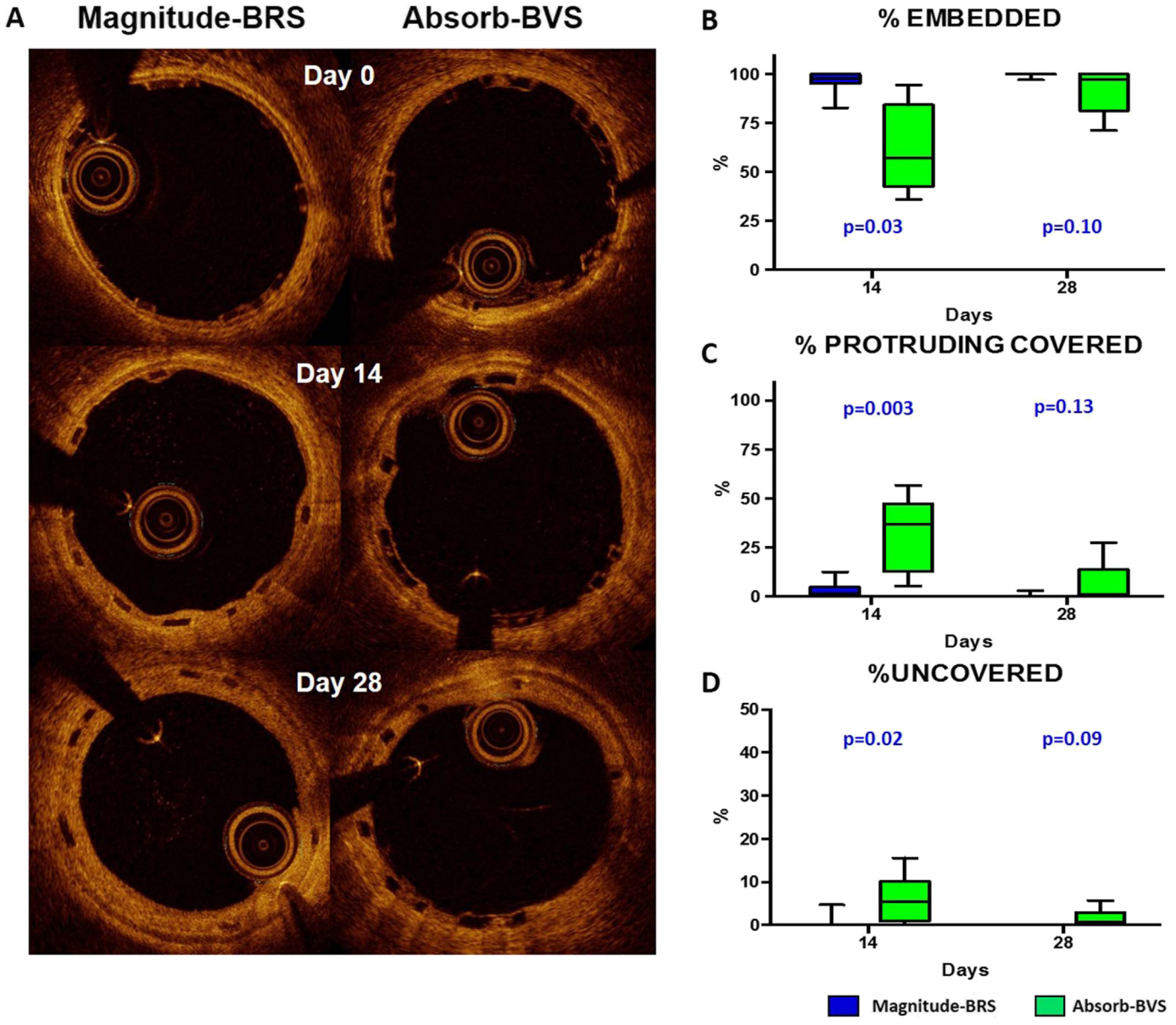

Fig. 1. Comparison of serial OCT variables at 14 and 28 days follow-up between Magnitude-BRS and Absorb-BVS. There was higher percentage of embedded struts at 14 days in the Magnitude-BRS group, while more uncovered struts were observed in the Absorb-BVS group at 14 days. Variables are expressed as median (25th–75th percentile).

Table 2
Optical coherence tomography data.

	Magnitude-BRS	Absorb-BVS	*p*
Day 0 (22 animals)	n = 43	n = 22	
Lumen area (mm^2)	6.79 ± 1.05	6.73 ± 8.18	0.89
Abluminal scaffold area (mm^2)	7.74 ± 1.13	8.18 ± 1.69	0.35
Day 28 (22 animals)	n = 43	n = 22	
Lumen area (mm^2)	4.89 ± 1.24	4.93 ± 1.49	0.92
Endoluminal scaffold area (mm^2)	6.64 ± 1.13	6.24 ± 1.37	0.24
Abluminal scaffold area (mm^2)	7.56 ± 1.24	7.63 ± 1.52	0.86
Area stenosis, (%)	35.8 ± 9.6	36.3 ± 9.5	0.86
Absolute scaffold recoil (mm^2)	−0.07[−0.32, 0.24]	0.24[−0.05, 0.72]	0.04
Percent scaffold recoil (%)	−1.02[−4.11, 3.21]	4.42[−1.10, 8.74]	0.04
Day 90 (16 animals)	n = 31	n = 16	
Lumen area (mm^2)	4.61 ± 1.13	4.78 ± 1.29	0.65
Endoluminal scaffold area (mm^2)	6.62 ± 1.12	6.35 ± 1.49	0.53
Abluminal scaffold area (mm^2)	7.56 ± 1.22	7.78 ± 1.64	0.65
Area stenosis, (%)	39.4 ± 9.0	38.9 ± 7.3	0.84
Absolute scaffold recoil (mm^2)	−0.02 [−0.42, 0.40]	0.44 [−0.24, 0.48]	0.27
Percent scaffold recoil (%)	−0.22 [−5.86, 5.52]	6.05 [−2.53, 7.56]	0.29
Day 180 (10 animals)	n = 19	n = 10	
Lumen area (mm^2)	4.98 ± 1.07	4.51 ± 0.57	0.13
Endoluminal scaffold area (mm^2)	6.97 ± 1.15	6.02 ± 0.72	0.03
Abluminal scaffold area (mm^2)	7.87 ± 1.27	7.39 ± 0.83	0.23
Area stenosis, (%)	36.9 ± 7.7	38.9 ± 5.6	0.44
Absolute scaffold recoil (mm^2)	−0.05 [−0.58, 0.33]	0.78 [0.10, 0.94]	0.049
Percent scaffold recoil (%)	−0.72 [−8.14, 3.90]	9.49 [1.56, 10.78]	0.052

Values are expressed as Mean ± SD or median (25th–75th percentile).

scaffolds to the sub-100 μm level without compromising the total vessel coverage area (21% to 25%) in all devices ranges (2.5 to 3.5 mm).

The impact of strut thickness on strut's healing and neointimal proliferation has been well described. Studies of coronary flow dynamics suggest that strut thickness and geometrical shape induces laminar flow disturbances around the struts' area due to the bigger device's footprint exposed to the vessel's surface potentially increasing the thrombogenicity of the device [11,12]. Recently published randomized trials with a follow-up of ≥2 years demonstrated higher risk of stent thrombosis and of target lesion failure in patients treated with BVS compared with everolimus-eluting stent [5,6]. The causes of scaffold thrombosis in both the early and late phases have yet to be fully elucidated. It is believed that bulky strut thickness promotes a pro- thrombotic environment specially when the device is either not properly implanted or delivered in small vessels [13]. As it happened in the drug-eluting stent field, it is expected that the scaffold thrombosis rates will decrease as the technology evolves and strut thickness decreases. An important objective of this study was the evaluation of the impact of strut thickness on early vascular healing by using OCT analysis over the first month. Our results showed that the Magnitude demonstrated superior strut coverage in early phase of vessel healing compared to Absorb. At 28-days, uncovered struts were still present in the Absorb group while complete strut coverage was documented by OCT at 14-days in the Magnitude group. Histological analysis showed comparable injury and peri-strut inflammation responses between both devices at all time points (Table 3).

One of the main challenges of BRS has been their limited ability to resist vessel recoil over time and under extreme loading conditions. Although clinically available BRS display acute radial forces comparable to metallic stents right after deployment, their ability to maintain lumen stability under specific biological conditions (i.e., calcium) has been questioned [14]. Optimal BRS design should ensure not only proper acute lumen gain but also to maintain long-term lumen patency as the vessel heals. Early clinical reports suggest that early scaffold dismantling resulting in intra-luminal strut protrusion may be responsible for target vessel failures and scaffold thrombosis [15]. In this study, at 6 months, incidental neointima-covered localized strut discontinuities were observed by histological evaluation, but all of them were focal, fully apposed to the vessel wall and covered with neointima, thus considered a normal manifestation of scaffold resorption resulting from polymer's molecular weight loss expected at this time point in both scaffold types. Post-implantation acute scaffold recoil was comparable between two devices. In the Magnitude-BRS group, there was no scaffold area decrease or late recoil observed at 6 months. Conversely, the Absorb group displayed slightly higher late absolute and percent recoil rates (Table 2), demonstrating that the tested BRS provided a more stable device dismantling process and superior longer-term architectural stability compared to Absorb.

4.1. Limitations

The present study has some limitations that are important to discuss. First, the in-vitro cyclic testing was performed in the straight model. The fatigue of coronary artery stents is mainly caused by contractions of the heart and strut fracture is closely related to the hinge motion of the implanted arteries. A recent study suggests that a change in the natural tortuous course of the coronaries by stent implantation with the decrease in coronary bending angle is a potentially major contributor in stent failure [16] However, the bench testing model used in this study did not evaluate the effect of vascular dynamic bending on stent mechanical properties, which has a significant impact on the stent's fatigue performance and should be considered when analyzing stent's long-term mechanical properties. In addition, the study was performed in healthy coronary arteries in the swine model of restenosis. All scaffolds were implanted in the main coronary artery segments avoiding large

Table 3
Histological data.

	Day 28 (6 animals)			Day 90 (6 animals)			Day 180 (10 animals)		
	Magnitude-BRS (n = 12)	Absorb-BVS (n = 6)	*p*	Magnitude-BRS (n = 12)	Absorb-BVS (n = 6)	*p*	Magnitude-BRS (n = 19)	Absorb-BVS (n = 10)	*p*
EEL (mm^2)	8.59 ± 1.09	8.31 ± 1.60	0.71	8.22 ± 1.49	9.67 ± 2.21	0.19	9.30 ± 1.59	8.75 ± 1.09	0.28
IEL (mm^2)	7.59 ± 0.96	7.21 ± 1.48	0.58	7.33 ± 1.33	8.44 ± 1.84	0.23	8.33 ± 1.37	7.70 ± 0.99	0.17
LA (mm^2)	5.56 ± 1.00	5.09 ± 1.52	0.51	4.68 ± 1.15	5.65 ± 1.58	0.22	5.64 ± 1.50	5.04 ± 1.07	0.23
NIT (mm)	0.23 ± 0.06	0.25 ± 0.05	0.42	0.31 ± 0.15	0.30 ± 0.07	0.88	0.30 ± 0.09	0.30 ± 0.06	0.82
% AS	27.0 ± 6.6	30.6 ± 8.1	0.38	35.7 ± 12.7	33.8 ± 8.9	0.72	32.9 ± 9.8	35.0 ± 7.2	0.52
Inflammation score	0.00 (0.00–0.00)	0.30 (0.08–0.60)	0.12	0.00 (0.00–0.48)	0.70 (0.40–1.15)	0.64	0.00 (0.00–0.85)	0.15 (0.00–1.22)	0.76
Injury score	1.00 (0.60–1.08)	0.15 (0.00–0.83)	0.054	0.70 (0.23–1.08)	0.65 (0.30–1.23)	0.64	0.70 (0.30–2.00)	1.30 (0.30–1.30)	0.78
Fibrin score	1.30 (1.00–1.70)	1.50 (1.00–2.00)	0.61	0.30 (0.00–0.30)	0.70 (0.18–0.70)	0.12	0.00 (0.00–0.30)	0.00 (0.00–0.00)	0.56
Neointimal maturity	3.00 (2.93–3.00)	2.85 (2.70–3.00)	0.28	3.00 (3.00–3.00)	3.00 (3.00–3.00)	1.00	3.00 (3.00–3.00)	3.00 (3.00–3.00)	1.00

Values are expressed as Mean ± SD or median (25th–75th percentile). EEL: external elastic lamina; IEL: the internal elastic lamina; LA: lumen area; NIT: neointimal thickness; AS: area stenosis.

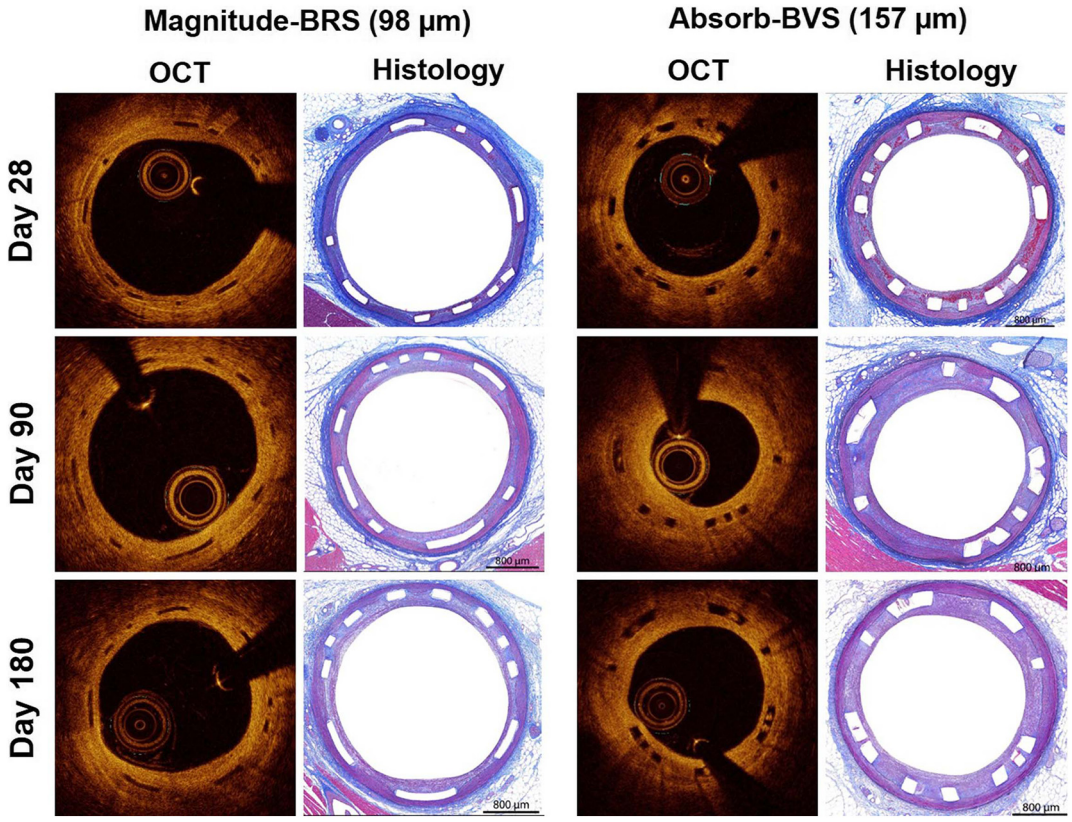

Supplementary Fig. 5. Representative matched histological and OCT images of the Magnitude-BRS and Absorb-BVS in porcine coronary arteries at 1, 3 and 6 months after implantation.

side branches (>2.0 mm). Therefore, although our data supports the safety and biocompatibility of the device, our findings cannot predict its clinical performance among patients with high atherosclerotic burden. However, in vitro, animal, and First-in-Human 9 month OCT data (TCT 2017, Granada J) suggest that the BRS tested in this study displays an acute biomechanical behavior comparable to metallic stents. The long-term biomechanical behavior of this device is currently under evaluation in a multicenter First-in-Human clinical investigation and long-term animal studies. Finally, although the 6-month follow up period presented in this study is sufficient to test the performance and safety of the device, a longer follow up period is required to evaluate the impact of polymer resorption on vascular healing and remodeling.

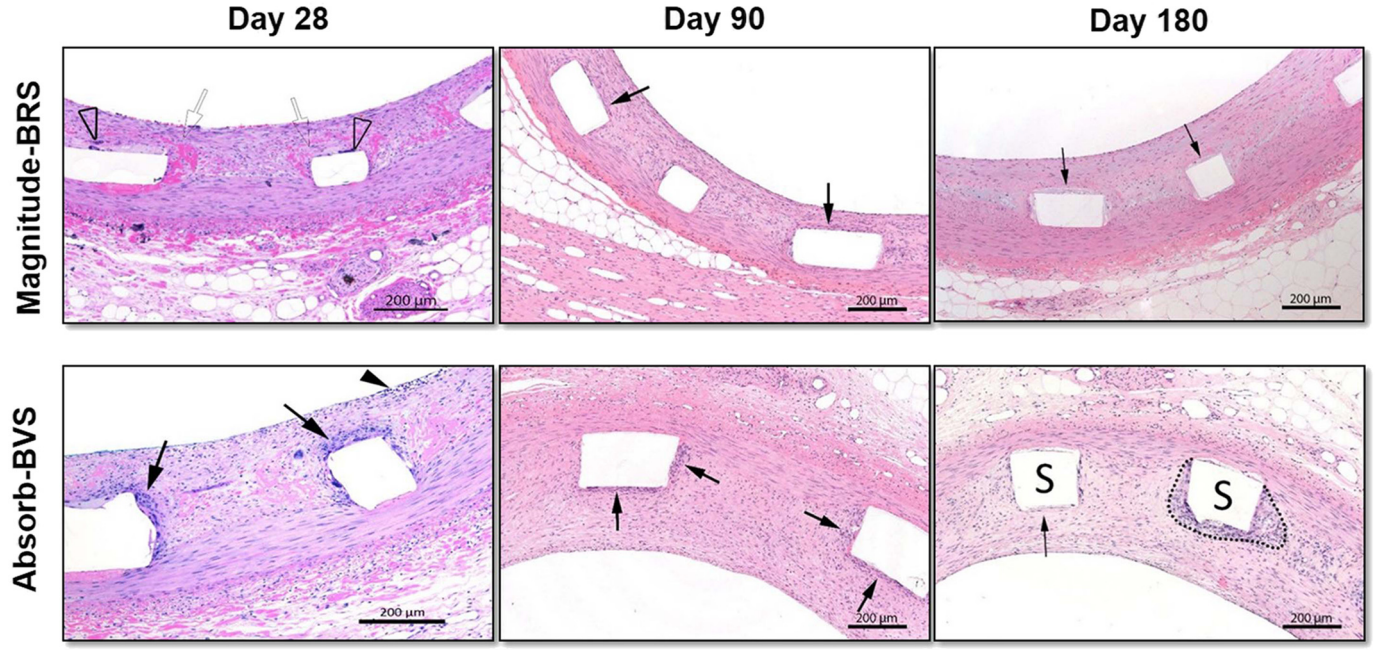

Supplementary Fig. 6. Histological images (H&E) show none to minimal inflammatory response around the scaffold struts at 1, 3 and 6 months. Arrows = none or minimal peristrut inflammation; Clear arrows = lack of inflammation response along the struts; Clear arrowheads = rare foreign body giant cells along the struts; Arrowhead = minimal focal inflammation in the superficial neointima; and Dotted line = slight and localized peristrut inflammation.

5. Conclusion

In conclusion, our data indicate that the novel thin strut (98 μm) sirolimus-eluting Magnitude-BRS demonstrated similar inhibition of neointimal proliferation with superior strut coverage at early follow-up compared to first-generation benchmark Absorb-BVS, maintaining vessel lumen stability during the 6-month follow-up period. Our findings suggest that the novel BRS tested in this study has the potential to improve the performance shown by the current generation BRS by providing a highly biocompatible and mechanically durable platform with radically decreased strut thickness.

Supplementary data to this article can be found online at https://doi.org/10.1016/j.ijcard.2019.04.012.

Acknowledgement of grant support

This study was funded by Amaranth Medical, Inc.

Conflict of interest statement

Authors Kamal Ramzipoor and Chang Lee were employees of Amaranth Medical, Inc. (Mountain View, CA). Juan F. Granada was a scientific advisor of Amaranth Medical, Inc. There are no other financial arrangements or other relationships that could be construed as a conflict of interest.

References

[1] S.G. Ellis, D.J. Kereiakes, D.C. Metzger, et al., Everolimus-eluting bioresorbable scaffolds for coronary artery disease, N. Engl. J. Med. 373 (2015) 1905–1915.
[2] P.W. Serruys, B. Chevalier, Y. Sotomi, et al., Comparison of an everolimus-eluting bioresorbable scaffold with an everolimus-eluting metallic stent for the treatment of coronary artery stenosis (ABSORB II): a 3 year, randomised, controlled, single-blind, multicentre clinical trial, Lancet 388 (2016) 2479–2491.
[3] N. Foin, R. Lee, A. Mattesini, et al., Bioresorbable vascular scaffold overexpansion: insights from in vitro post-expansion experiments, EuroIntervention 11 (2016) 1389–1399.
[4] G.W. Stone, J.F. Granada, Very late thrombosis after bioresorbable scaffolds: cause for concern? J. Am. Coll. Cardiol. 66 (2015) 1915–1917.
[5] R.A. Montone, G. Niccoli, F. De Marco, et al., Temporal trends in adverse events after everolimus-eluting bioresorbable vascular scaffold versus everolimus-eluting metallic stent implantation: a meta-analysis of randomized controlled trials, Circulation 135 (2017) 2145–2154.
[6] J.J. Wykrzykowska, R.P. Kraak, S.H. Hofma, et al., Bioresorbable scaffolds versus metallic stents in routine PCI, N. Engl. J. Med. 376 (2017) 2319–2328.
[7] T.P. Vahl, P. Gasior, C.A. Gongora, et al., Four-year polymer biocompatibility and vascular healing profile of a novel ultrahigh molecular weight amorphous PLLA bioresorbable vascular scaffold: an OCT study in healthy porcine coronary arteries, EuroIntervention 12 (2016) 1510–1518.
[8] Y. Cheng, P. Gasior, M. Shibuya, et al., Comparative characterization of biomechanical behavior and healing profile of a novel ultra-high-molecular-weight amorphous poly-L-lactic acid sirolimus-eluting bioresorbable coronary scaffold, Circ. Cardiovasc. Interv. 12 (2016) 1164–1173.
[9] Y. Cheng, P. Gasior, J.G. Xia, et al., Comparative biomechanical behavior and healing profile of a novel thinned-wall ultrahigh molecular weight amorphous poly-L-lactic acid sirolimus-eluting bioresorbable coronary scaffold, Circ. Cardiovasc. Interv. 10 (7) (2017), e005116.
[10] H. Kawamoto, V.F. Panoulas, K. Sato, et al., Impact of strut width in periprocedural myocardial infarction: a propensity-matched comparison between bioresorbable scaffolds and the first-generation sirolimus-eluting stent, JACC Cardiovasc. Interv. 8 (2015) 900–909.
[11] K.C. Koskinas, Y.S. Chatzizisis, A.P. Antoniadis, G.D. Giannoglou, Role of endothelial shear stress in stent restenosis and thrombosis: pathophysiologic mechanisms and implications for clinical translation, J. Am. Coll. Cardiol. 59 (2012) 1337–1349.
[12] B.D. Gogas, S.B. King 3rd, L.H. Timmins, et al., Biomechanical assessment of fully bioresorbable devices, JACC Cardiovasc. Interv. 6 (2013) 760–761.
[13] Y. Sotomi, P. Suwannasom, P.W. Serruys, Y. Onuma, Possible mechanical causes of scaffold thrombosis: insights from case reports with intracoronary imaging, EuroIntervention 12 (2017) 1747–1756.
[14] A. Mattesini, G.G. Secco, G. Dall'Ara, et al., ABSORB biodegradable stents versus second-generation metal stents: a comparison study of 100 complex lesions treated under OCT guidance, JACC Cardiovasc. Interv. 7 (2014) 741–750.
[15] L. Azzalini, P.L. L'Allier, Bioresorbable vascular scaffold thrombosis in an all-comer patient population: single-center experience, J. Invasive Cardiol. 27 (2015) 85–92.
[16] B.C. Zhang, S.X. Tu, A. Karanasos, et al., Association of stent-induced changes in coronary geometry with late stent failure: insights from three-dimensional quantitative coronary angiographic analysis, Catheter. Cardiovasc. Interv. 92 (2018) 1040–1048.